Electromagnetic wave propagation through doubly dispersive subwavelength metamaterial hole

Ki Young Kim[1], Jeong-Hae Lee[2], Young Ki Cho[1], and Heung-Sik Tae[1]

[1]*School of Electrical Engineering and Computer Science, Kyungpook National University, Daegu 702-701, Korea*
[2]*Department of Radio Science and Communication Engineering, Hongik University, Seoul 121-791, Korea*
doors@ee.knu.ac.kr

http://palgong.knu.ac.kr/~doors

Abstract: The characteristics of the guided electromagnetic wave propagation through a subwavelength hole surrounded by a doubly dispersive metamaterial are investigated. Characteristic equations are derived for the surface polariton modes related to the subwavelength hole and mode classifications established. The surface polariton modes for two different hole-radii are numerically obtained and their electromagnetic dispersion curves and power flux characteristics analyzed and compared with each other. In particular, it was found that the border of the counter-propagation between the forward and backward Poynting vectors was located within the metamaterial, rather than at the interface between the metamaterial and the free space.

OCIS codes: (130.2790) Guided waves; (240.5420) Polaritons; (240.6680) Surface plasmons; (260.2030) Dispersion; (350.5500) Propagation.

References and links

1. T. Thio, K. M. Pellerin, R. A. Linke. H. J. Lezec, and T. W. Ebbesen, "Enhanced light transmission through a single subwavelength aperture," Opt. Lett. **26**, 1972-1974 (2001).
2. H. J. Lezec, A. Degiron, E. Devaux, R. A. Linke, L. Martin-Moreno, F. J. Garcia-Vidal, T. W. Ebbesen, "Beaming light from a subwavelength aperture," Science **297**, 820-822 (2002).
3. L. Martín-Moreno, F. J. García-Vidal, H. J. Lezec, A. Degiron, and T. W. Ebbesen, "Theory of highly directional emission from a single subwavelength aperture surrounded by surface corrugations," Phys. Rev. Lett. **90**, 167401 (2003).
4. F. J. García-Vidal, H. J. Lezec, T. W. Ebbesen, and L. Martín-Moreno, "Multiple paths to enhance optical transmission through a single subwavelength slit," Phys. Rev. Lett. **90**, 213901 (2003).
5. A. Degiron and T. W. Ebbesen, "Analysis of the transmission process through single apertures surrounded by periodic corrugations," Opt. Express **12**, 3694-3670 (2004), http://www.opticsexpress.org/abstract.cfm?URI=OPEX-12-16-3694
6. A. Degiron, H. J. Lezec, N. Yammamoto, and T. W. Ebbesen, "Optical transmission properties of a single subwavelnegth aperture in a real metal," Opt. Commun. **239**, 61-64 (2004).
7. N. Bonod, E. Popov, and M. Nevière, "Light transmission through a subwavelength microstructured aperture: electromagnetic theory and applications," Opt. Commun. **245**, 355-361 (2005).
8. A. V. Klyuchnik, S. Y. Kurganov, and Y. E. Lozovik, "Plasma optics of nanostructures," Phys. Solid State **45**, 1327-1331 (2003).
9. H. Raether, Surface Plasmons on Smooth and Rough Surfaces and on Gratings, (Springer-Verlag, 1988).
10. D. R. Smith, W. J. Padilla, D. C. Vier, S. C. Nemat-Nasser, and S. Schultz, "Composite medium with simultaneously negative permeability and permittivity," Phys. Rev. Lett. **84**, 4184-4187 (2000).
11. R. Ruppin, "Surface polaritons of a left-handed medium," Phys. Lett. A **277**, 61-64 (2000).
12. R. Ruppin, "Surface polaritons of a left-handed material slab," J. Phys.: Condens. Matter **13** 1811-1819 (2001).
13. H. O. Moser, B. D. F. Casse, O. Wilhelmi, and B. T. Saw, "Terahertz response of a microfabricated rod-split-ring-resonator electromagnetic metamaterial," Phys. Rev. Lett. **94**, 063901 (2005).
14. I. V. Shadrivov, A. A. Sukhorukov, and Y. S. Kivshar, "Guided modes in negative-refractive-index waveguides," Phys. Rev. E **67**, 057602 (2003).

#7129 - $15.00 US Received 12 April 2005; revised 1 May 2005; accepted 1 May 2005

15. H. Dong and T. X. Wu, "Analysis of discontinuities in double-negative (DNG) slab waveguides," Microwave Opt. Tech. Lett. **39**, 483-488 (2003).
16. H. Cory and A. Barger, "Surface-wave propagation along a metamaterial slab," Microwave Opt. Tech. Lett. **38**, 392-395 (2003).
17. B. –I. Wu, T. M. Grzegorczyk, Y. Zhang, and J. A. Kong, "Guided modes with imaginary transverse wave number in a slab waveguide with negative permittivity and permeability," J. Appl. Phys. **93**, 9386-9388 (2003).
18. P. Baccarelli, P. Burghignoli, G. Lovat, and S. Paulotto, "Surface-wave suppression in a double-negative metamaterial grounded slab," IEEE Ant. Wireless Prop. Lett. **2**, 269-272 (2003).
19. M. M. B. Suwailiam, Z. Chen, "Surface waves on a grounded double-negative (DNG) slab waveguide," Microwave Opt. Tech. Lett. **44**, 494-498 (2005).
20. J. Schelleng, C. Monzon, P. F. Loschialpo, D. W. Forester, and L. N. Medgye-Mitschang, "Characteristics of waves guided by a grounded "left-handed" material slab of finite extent," Phys Rev E **70**, 066606 (2004).
21. A. C. Peacock and N. G. R. Broderick, "Guided modes in channel waveguides with a negative index of refraction," Opt. Express **11** , 2502-2510 (2003), http://www.opticsexpress.org/abstract.cfm?URI=OPEX-11-20-2502
22. A. V. Novitsky and L. M. Barkovsky, "Guided modes in negative-refractive-index fibres," J. Opt. A: Pure Appl. Opt **7**, S51-S56 (2005).
23. H. Cory and T. Blum, Surface-wave propagation along a metamaterial cylindrical guide, Microwave Opt. Tech. Lett. **44**, 31-35 (2005).
24. K. Y. Kim, Guided and Leaky Modes of Circular Open Electromagnetic Waveguides: Dielectric, Plasma, and Metamaterial Columns, Ph.D. Thesis, Kyungpook National University, (2004), http://palgong.knu.ac.kr/~doors/PDFs/PhDThesis.pdf
25. A. Safaai-Jazi and G. L .Yip, "Classification of hybrid modes in cylindrical dielectric optical waveguides," Radio Sci. **12**, 603-609 (1977).
26. V. L .Granatstein, S. P. Schlesinger, and A. Vigants, "The open plasmaguide in extreme of magnetic field," IEEE Trans. Ant. Prop. **11**, 489-496 (1963).
27. V. G. Veselago, "The electrodynamics of substances with simultaneously negative values of ε and μ," Sov. Phys. Usp. **10**, 509-514 (1968).
28. K. Halterman, J. M. Elson, and P. L. Overfelt, "Characteristics of bound modes in coupled dielectric waveguides containing negative index media," Opt. Express **11**, 521-529 (2003), http://www.opticsexpress.org/abstract.cfm?URI=OPEX-11-6-521
29. A. A. Oliner and T. Tamir, "Backward waves on isotropic plasma slabs," J. Appl. Phys. **33**, 231-233 (1962)
30. T. Tamir and S. Palócz, "Surface waves on plasma-clad metal rods," IEEE Trans. Microwave Theory Tech. **12**, 189-196 (1964).
31. I. V. Shadrivov, A. A. Sukhorukov, Y. S. Kivshar, A. A. Zharov, A. D. Boardman, and P. Egan, "Nonlinear surface waves in left-handed materials," Phys. Rev. E **69**, 016617 (2004)

1. Introduction

Extraordinary enhanced optical transmission though a single subwavelength aperture in metal structures has been receiving much attention [1-7] due to its unexpected behavior in relation to conventional theories and potential application in such areas as high density optical data storage, near field optical microscopy, subwavelength lithography, optical sensors, and optical displays. One plausible explanation for this phenomenon is the excitation of the surface polariton (SP) mode from the incident light at the entrance aperture, propagation of the SP mode through the subwavelength metal structure with a finite thickness or length, and de-excitation of the SP mode into the emitted light at the exit aperture [8]. In principle, the efficiency of the throughput is dependent on the conversion efficiency between the SP mode and the incident (and emitted) light. In general, SP mode propagation is known to exist at the interface between metals and dielectrics [9], where the permittivity of the metal is negative at a given frequency and plays a crucial role in the SP mode propagation through the subwavelength metal structure. If we assume that the frequency dependent behavior of a metal at optical frequencies as the well known Drude model, *i.e.*, $\varepsilon_m = \varepsilon_0 \left(1 - \omega_p^2 / \omega^2\right)$, where ε_0 is the permittivity of the free space and ω_p is the plasma frequency of the angular form, the permittivity of a metal is negative below the plasma frequency and also frequency dispersive. Klyuchnik *et al.* already showed the existence of SP modes along a subwavelength cylindrical metal cavity, and briefly examined the dispersion properties of the SP eigenmodes due to the frequency dispersive character of the metal [8].

#7129 - $15.00 US Received 12 April 2005; revised 1 May 2005; accepted 1 May 2005

Recently, there has been a rapid growth of interest in metamaterials (MTMs), which are engineered artificial electromagnetic substances whose permittivity and permeability are simultaneously negative at a given desired frequency [10]. Ruppin also demonstrated the existence of an SP mode at the interface between an MTM and normal dielectric material [11, 12]. The SP modes on an MTM are expected to have multiple applications within a broad frequency spectrum, as an MTM can be artificially designed from microwave [10] to terahertz frequencies [13] or above. Therefore, even though current fabrication techniques of isotropic MTMs are still in the early stage of development, a theoretical analysis of the electromagnetic wave propagation along an MTM subwavelength hole is worthwhile to provide the guided mode characteristics of other fundamental simple guiding structures with MTMs, such as slabs [14-17], grounded slabs [18-20], channels [21], and cylinders [22-24].

Accordingly, the present study investigates the electromagnetic wave propagation along a subwavelength circular hole surrounded by a doubly dispersive metamaterials (DDMTM). The field components are defined and used to derive the characteristic equations. The mode classifications are then made and the electromagnetic dispersions and power flux characteristics of two different diametric holes surrounded by a DDMTM analyzed and compared.

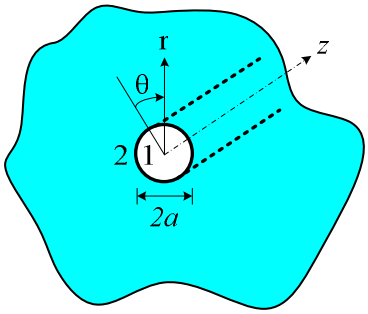

Fig. 1. Schematic view of subwavelength DDMTM hole with diameter $D = 2a$ in cylindrical coordinate system. The inner and outer regions are the free space (region 1) and DDMTM (region 2), respectively.

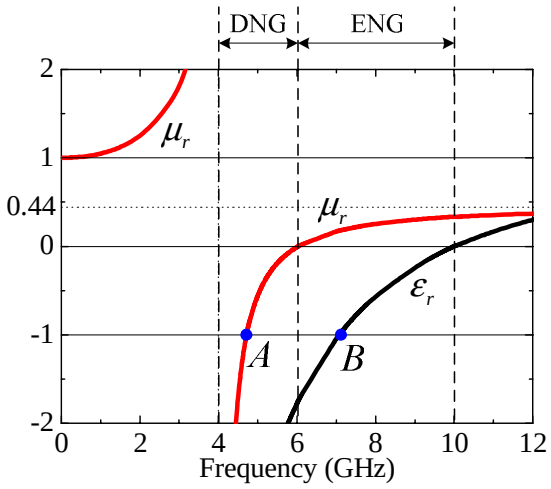

Fig. 2. Material constants of DDMTM. The DNG and ENG regions are from 4 to 6 GHz and 6 to 10 GHz, respectively.

#7129 - $15.00 US
Received 12 April 2005; revised 1 May 2005; accepted 1 May 2005

2. Field components, characteristic equations, and power fluxes

2.1 Subwavelength hole surrounded by doubly dispersive metamaterial

Figure 1 shows a schematic view of the subwavelength hole surrounded by a DDMTM. The inner and surrounding regions are the free space (region 1) and DDMTM (region 2), respectively. The diameter of the hole is depicted as $D = 2a$, where a is the radius. The free space region is characterized by $\varepsilon_{r1} = \mu_{r1} = 1.0$ and the relative permittivity and permeability of the DDMTM can be respectively assumed as follows:

$$\varepsilon_{r2}(\omega) = 1 - \frac{\omega_p^2}{\omega^2} \tag{1a}$$

$$\mu_{r2}(\omega) = 1 - \frac{F\omega^2}{\omega^2 - \omega_0^2} \tag{1b}$$

where ω_0 is the resonant frequency of the angular form. The assumed MTM parameters are $\omega_p / 2\pi = 10$ GHz, $\omega_0 / 2\pi = 4$ GHz, and $F = 0.56$, based on the experimental values of a structure composed of metallic rods and split ring resonators (SRRs) [10], plus these parameters have also been used in other studies on isotropic MTMs [11, 12, 14, 21, 22, 24]. Figure 2 shows plots of the material expressions of Eq. (1). When using the selected parameters, the relative permittivity and permeability are both negative in the region from 4 to 6 GHz, called the double negative (DNG) region. Meanwhile, only the permittivity is negative in the region from 6 to 10 GHz, called the epsilon-negative (ENG) region. Since no SP mode solutions were found between $f < 4$ GHz and $f > 10$ GHz, those frequency regions are disregarded. Instead, the frequencies marked at *A* (4.714 GHz) and *B* (7.071 GHz) are the critical frequencies playing an important role in the dispersion relation, and will be discussed in section 3.

2.2 Field expressions

Since electromagnetic fields from an open guiding structure are vanish at infinity, a modified Bessel function of the second kind, *i.e.*, $K_m(k_2 r)$, is selected to express the behavior of the axial electric and magnetic fields along the transverse direction (*r*) in the DDMTM region, where *m* is the azimuthal eigenvalue and k_2 is the transverse propagation constant in the DDMTM region. If $K_m(k_2 r)$ is chosen as the surrounding field, k_2 is given as $k_2 = \left(\beta^2 - k_0^2 \mu_{r2} \varepsilon_{r2}\right)^{1/2}$ [25], where β and k_0 are the axial propagation constant and free space wave number, respectively. For the DNG case, *i.e.*, $\mu_{r2} < 0$ and $\varepsilon_{r2} < 0$, the condition for the square root to be positive is $\overline{\beta} = \beta / k_0 > \left(\mu_{r2} \varepsilon_{r2}\right)^{1/2}$, where $\overline{\beta}$ is the normalized propagation constant. In contrast, the single negative (SNG) material constants themselves, *i.e.*, $\mu_{r2} > 0$ and $\varepsilon_{r2} < 0$ (ENG), or $\mu_{r2} < 0$ and $\varepsilon_{r2} > 0$ (mu-negative (MNG)), are sufficient condition for the square root to be positive. Nonetheless, the condition $\beta / k_0 > \left(\mu_{r1} \varepsilon_{r1}\right)^{1/2} \left(= 1.0\right)$ for the free space region (region 1) needs to be simultaneously satisfied to support the slow waves in this structure. Thus, the transverse propagation constants in the free space region can be expressed as $k_1 = \left(\beta^2 - k_0^2 \mu_{r1} \varepsilon_{r1}\right)^{1/2}$ and the proper choice of a Bessel function for the free space region needs to be a modified Bessel function of the first kind, *i.e.*, $I_m(k_1 r)$ [25]. Therefore, in the DNG region, the allowed SP mode solutions for $\overline{\beta}$ must be within the region of $\overline{\beta} > \left(\mu_{r2} \varepsilon_{r2}\right)^{1/2}$ and $\overline{\beta} > \left(\mu_{r1} \varepsilon_{r1}\right)^{1/2}$ for

#7129 - $15.00 US
Received 12 April 2005; revised 1 May 2005; accepted 1 May 2005

$(\mu_{r2}\varepsilon_{r2})^{1/2} > (\mu_{r1}\varepsilon_{r1})^{1/2} (=1.0)$ and $(\mu_{r1}\varepsilon_{r1})^{1/2} (=1.0) > (\mu_{r2}\varepsilon_{r2})^{1/2}$, respectively. Resultant axial fields of the DDMTM hole are identical to those for a plasma column [26] and the SP mode of an MTM column [22-24]. Figure 3 shows the allowed SP mode region of the DDMTM hole for the DNG and SNG cases. In the SNG region, only $\bar{\beta} > (\mu_{r1}\varepsilon_{r1})^{1/2}$.

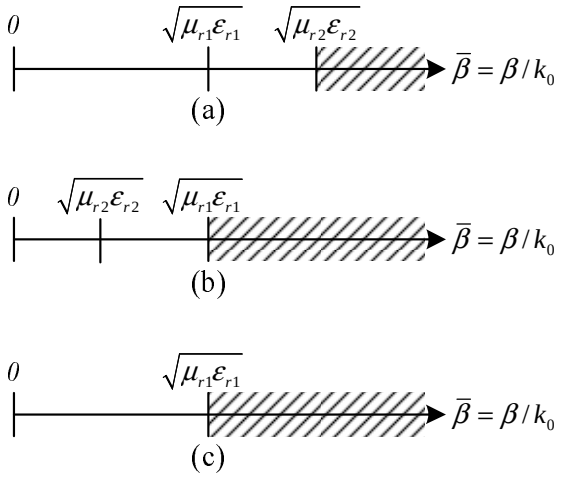

Fig. 3. Allowed SP mode region of DDMTM hole for DNG and SNG cases. (a) DNG with $\sqrt{\mu_{r2}\varepsilon_{r2}} > \sqrt{\mu_{r1}\varepsilon_{r1}}$, (b) DNG with $\sqrt{\mu_{r1}\varepsilon_{r1}} > \sqrt{\mu_{r2}\varepsilon_{r2}}$, and (c) SNG (ENG or MNG).

2.3 Characteristic equations

Following the standard steps of deriving characteristic equations using the fields described in the previous section, the general characteristic equation can be obtained as follows

$$\left[\frac{\varepsilon_{r1}}{k_1}\frac{I_m'(k_1a)}{I_m(k_1a)} - \frac{\varepsilon_{r2}}{k_2}\frac{K_m'(k_2a)}{K_m(k_2a)}\right]\left[\frac{\mu_{r1}}{k_1}\frac{I_m'(k_1a)}{I_m(k_1a)} - \frac{\mu_{r2}}{k_2}\frac{K_m'(k_2a)}{K_m(k_2a)}\right] = \left[\frac{m\beta}{k_0 a}\left(\frac{1}{k_1^2} - \frac{1}{k_2^2}\right)\right]^2. \qquad (2)$$

Prime denotes the differentiation. For $m = 0$, the characteristic equation (2) is split into two characteristic equations involving the TM_{0n} and TE_{0n} modes as follows, respectively:

$$\frac{\varepsilon_{r1}}{k_1}\frac{I_1(k_1a)}{I_0(k_1a)} + \frac{\varepsilon_{r2}}{k_2}\frac{K_1(k_2a)}{K_0(k_2a)} = 0 \qquad (3a)$$

$$\frac{\mu_{r1}}{k_1}\frac{I_1(k_1a)}{I_0(k_1a)} + \frac{\mu_{r2}}{k_2}\frac{K_1(k_2a)}{K_0(k_2a)} = 0. \qquad (3b)$$

In a more general case, *i.e.*, $m \geq 1$, the characteristic equation (2) can be written as follows using an empirical induction procedure:

$$\left(\frac{\mu_{r2}}{\mu_{r1}} + \frac{\varepsilon_{r2}}{\varepsilon_{r1}}\right)\frac{Q}{2} \pm \sqrt{\left\{\left(\frac{\mu_{r2}}{\mu_{r1}} + \frac{\varepsilon_{r2}}{\varepsilon_{r1}}\right)\frac{Q}{2}\right\}^2 + \frac{R}{\mu_{r1}\varepsilon_{r1}}} - P = 0 \qquad (4a)$$

where

#7129 - $15.00 US
Received 12 April 2005; revised 1 May 2005; accepted 1 May 2005

$$P = \frac{1}{k_1 a}\left(\frac{I_{m-1}(k_1 a)}{I_m(k_1 a)} - \frac{m}{k_1 a}\right) \tag{4b}$$

$$Q = -\frac{1}{k_2 a}\left(\frac{K_{m-1}(k_2 a)}{K_m(k_2 a)} + \frac{m}{k_2 a}\right) \tag{4c}$$

$$R = \left\{\frac{m\beta}{k_0 a^2}\left(\frac{1}{k_1^2} - \frac{1}{k_2^2}\right)\right\}^2 . \tag{4d}$$

Since the mode satisfying the characteristic equation (4) has both electric and magnetic fields in its axial components, the mode is called a hybrid mode. The " $\pm$ " signs in Eq. (4*a*) correspond to the HE_{mn} and EH_{mn} modes, respectively. The mode whose axial electric (magnetic) field is dominant is traditionally referred to as the HE_{mn} (EH_{mn}) mode. Plus, since the HE_{mn} (EH_{mn}) mode is similar to the TM_{0n} (TE_{0n}) mode, the modes such as TM_{0n}, HE_{1n}, HE_{2n}, $\cdots$ (TE_{0n}, EH_{1n}, EH_{2n}, $\cdots$) *etc*. are called the TM-like (TE-like) modes.

2.4 Power considerations

Backward waves can be supported in MTMs [27] due to the intrinsic left-handedness of MTMs. Thus, to analyze the backward wave characteristics, the present study considered the normalized power flux $\eta = (P_1 + P_2)/(|P_1| + |P_2|)$ [14, 21]. P_1 and P_2 are the fractional power fluxes in regions 1 and 2, respectively, and given as $P_1 = \int_0^a S_{z1}\, rdr$ and $P_2 = \int_a^\infty S_{z2}\, rdr$, respectively, where the axial components of the Poynting vectors in regions 1 and 2 can be given as $S_{z1} = E_{r1}H_{\theta 1}^* - E_{\theta 1}H_{r1}^*$ and $S_{z2} = E_{r2}H_{\theta 2}^* - E_{\theta 2}H_{r2}^*$, respectively. E_{ri} and $E_{\theta i}$ (H_{ri} and $H_{\theta i}$) ($i = 1, 2$) are the radial and azimuthal electric (magnetic) field components. Asterisk denotes the complex conjugate. Since P_1 and P_2 are expected to have opposite signs, $\eta > 0$ and $\eta < 0$ are the conditions for the forward and backward waves, respectively, where $\eta = 0$ means the cancellation of the power fluxes between the forward and backward waves. Moreover, a larger positive (negative) value for η implies a more tightly (loosely) bound mode in the free space region ($r < a$) of the subwavelength hole.

3. Numerical results and discussions

3.1 TE-like modes

Figure 4 shows the dispersion curves and their corresponding normalized power flux for the TE-like modes of the subwavelength hole with a 20.0 mm diameter. SP mode solutions existed above a frequency of 4.714 GHz, corresponding to point "*A*" in Fig. 2, where $\mu_{r2} = -1.0$, and all the SP mode solutions existed in the DNG region (4 to 6 GHz) in Fig. 2. In the case of an MTM column with identical MTM parameters to Eq. (1), all the guided mode solutions existed below this critical frequency [24]. It was also found that only a principal mode ($n = 1$) existed for each azimuthal eigenvalue, whereas higher order modes existed in the case of an MTM column. The negative slopes of the dispersion curves indicated the backward waves [26], which were also identified by the normalized power flux, *i.e.*, $\eta < 0$ as shown in Fig. 4(b). In the present study, all the TE-like SP mode solutions for the chosen parameters were backward wave type.

#7129 - $15.00 US Received 12 April 2005; revised 1 May 2005; accepted 1 May 2005

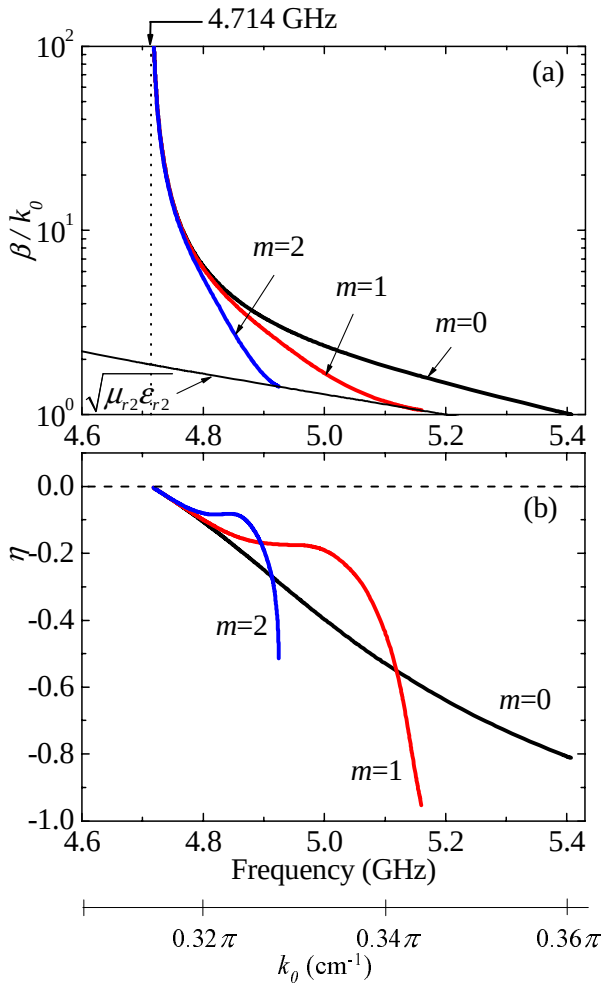

Fig. 4. TE-like modes of DDMTM hole with $D = 20.0$ mm . (a) Dispersion curves and (b) normalized power flux. Corresponding operating wave numbers are also shown.

The cutoff for the TE_{01} ($m = 0$) mode was on the $\beta / k_0 = 1.0$ line, while the cutoff frequency was 5.407 GHz, as in the case of Fig. 3(b), *i.e.*, $(\mu_{r1}\varepsilon_{r1})^{1/2} > (\mu_{r2}\varepsilon_{r2})^{1/2}$. In contrast, the cutoff for the hybrid modes, such as the EH_{11} ($m = 1$) and EH_{21} ($m = 2$) modes, was on the $\beta / k_0 = (\mu_{r2}\varepsilon_{r2})^{1/2}$ line, while the cutoff frequencies were 5.186 GHz and 4.925 GHz, respectively, as in the case of Fig. 3(a), *i.e.*, $(\mu_{r2}\varepsilon_{r2})^{1/2} > (\mu_{r1}\varepsilon_{r1})^{1/2}$. Thus, the single TE-like SP mode propagation region was from 5.186 to 5.407 GHz, with a width of 0.221 GHz. When analyzing the TE-like mode of the MTM subwavelength hole with a 20.0 mm diameter, the wavelengths of the obtained TE-like SP modes ranged from 55.48 mm (5.407 GHz) to 63.64 mm (4.714 GHz), representing approximately three times the diameter of the subwavelength hole.

#7129 - $15.00 US
Received 12 April 2005; revised 1 May 2005; accepted 1 May 2005

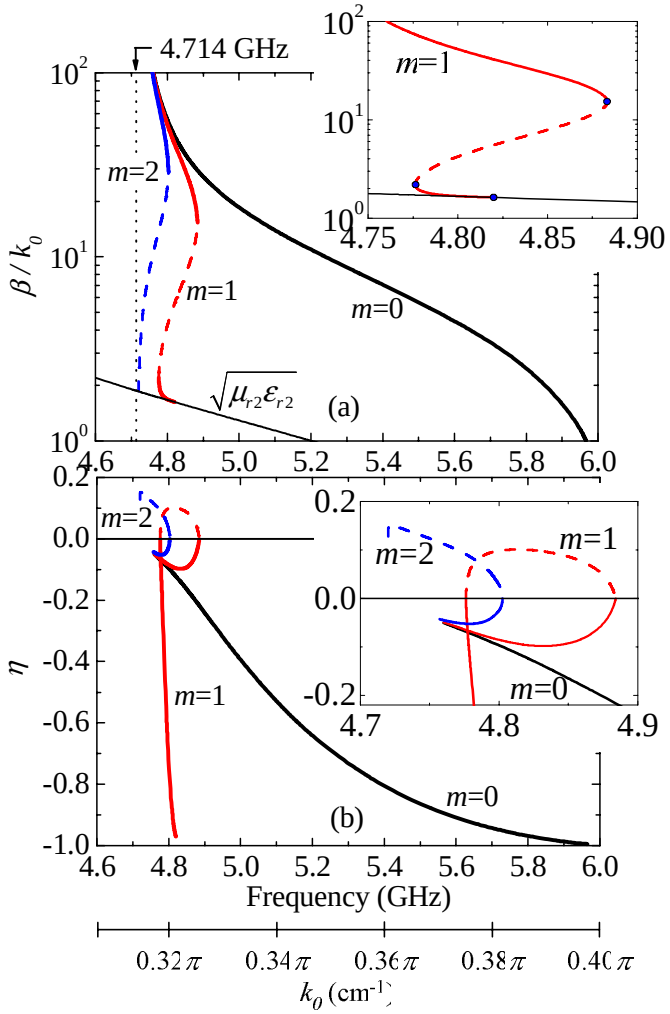

Fig. 5. TE-like modes of DDMTM hole with $D = 2.0$ mm . (a) Dispersion curves and (b) normalized power flux. Insets are enlarged scales. Corresponding operating wave numbers are also shown.

When considering a smaller subwavelength DDMTM hole with a 2.0 mm diameter, the dispersion curves and normalized power flux for the TE-like modes are shown in Fig. 5. The cutoff frequency for the TE_{01} mode shifted higher to 5.967 GHz (from 5.407 GHz in $D = 20.0$ mm case) and all the TE_{01} SP mode solutions were backward wave type. In contrast,
for the hybrid modes ($m \geq 1$), *i.e.*, the EH_{11} and EH_{21} modes, forward waves were generated, as designated by dashed lines in Fig. 5. The slopes of the forward waves in the dispersion curves were positive, and $\eta > 0$ for the corresponding region, as shown in Fig. 5(b). In spite of dissimilar geometrical configuration, forward and backward wave traveling properties associated with the respective positive and negative slopes in the dispersion curves of the MTM guiding structure were well described by Halterman *et al* [28]. Note that the forward waves of the EH_{m1} mode appeared with a small hole radius. However, in the case of a simple waveguide structure with frequency dispersive plasma media, such as a plasma slab [29],

#7129 - $15.00 US
Received 12 April 2005; revised 1 May 2005; accepted 1 May 2005

plasma column [26], and plasma Goubau line [30], small-sized waveguide cross sections produce backward waves from forward waves, which is the opposite to the present work.

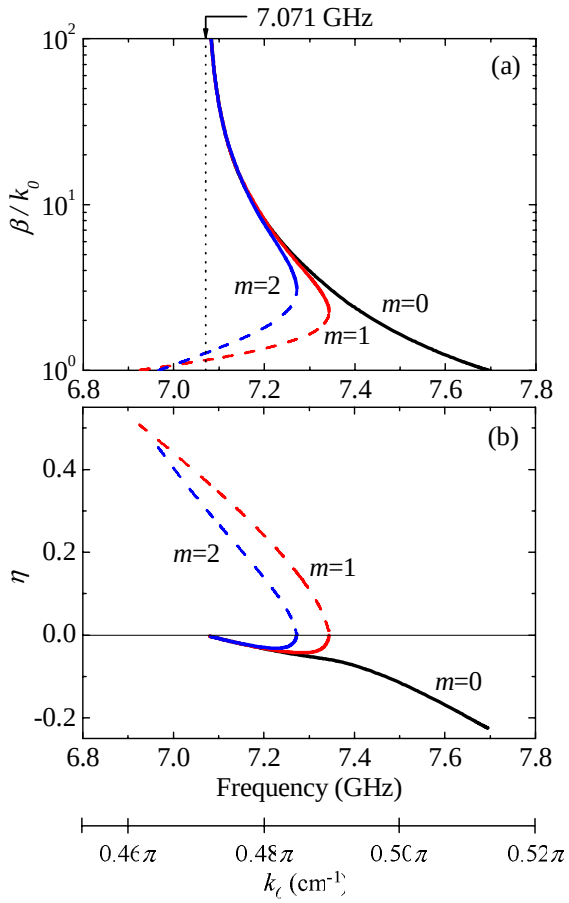

Fig. 6. TM-like modes of DDMTM hole with $D = 20.0$ mm . (a) Dispersion curves and (b) normalized power flux. Corresponding operating wave numbers are also shown.

The cutoff frequencies for the EH_{11} and EH_{21} modes on the $\beta / k_0 = (\mu_{r2}\varepsilon_{r2})^{1/2}$ line were 4.820 and 4.720 GHz, respectively. In the case of the EH_{11} mode, from 4.776 to 4.820 GHz, as shown in the inset of Fig. 5(a), three SP modes, *i.e.*, one forward wave and two backward waves were found to coexist, yet orthogonal to each other [15]. From 4.820 to 4.884 GHz, one forward wave and backward wave coexisted at the same frequency, and below 4.776 GHz, only a single backward wave existed that was limited to 4.714 GHz, which is the lower frequency limit for backward waves. Meanwhile, for the EH_{11} mode, the bifurcation frequency of 4.884 GHz was higher than the cutoff frequency of 4.820 GHz. Thus, only a single TE_{01} SP mode propagation was available from 4.884 to 5.967 GHz with a bandwidth of 1.083 GHz, which was broader than the previous case of $D = 20.0$ mm (0.221 GHz). As such, the wavelengths for the obtained TE-like SP modes in the case of $D = 2.0$ mm ranged from 50.28 mm (5.967 GHz) to 63.64 mm (4.714 GHz), representing approximately 30 times the diameter of the hole. The existence of the TE-like mode is due to the negative value of the permeability in the DNG region, which cannot be observed in a hole with ENG material surrounded. Thus, this DDMTM hole can be a potential applicant to a prove tip of a near-field

#7129 - $15.00 US
Received 12 April 2005; revised 1 May 2005; accepted 1 May 2005

microscope, which can scan specimens by use of the incident TE_{01} mode as well as TM_{01} mode, simultaneously or independently.

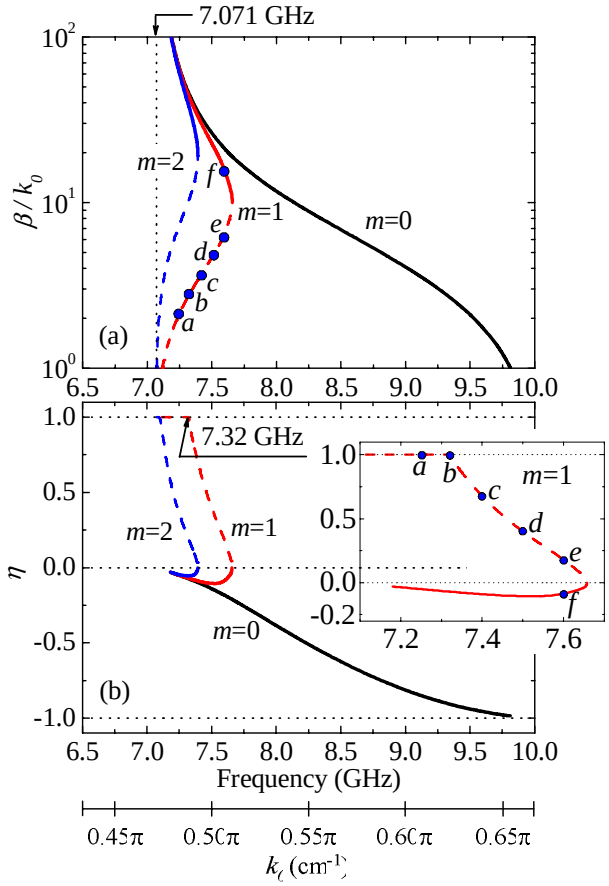

Fig. 7. TM-like modes of DDMTM hole with $D = 2.0$ mm . (a) Dispersion curves and (b) normalized power flux. The inset in (b) is an enlarged scale of the normalized power flux for the HE_{11} mode. At 7.32 GHz (point *b*), $\eta = 0$. Points *a*, *b*, *c*, *d*, *e*, and *f* indicate the positions of the plots of the Ponyting vectors S_{z1} and S_{z2} in Fig. 8.

3.2 TM-like modes

Figure 6 shows the dispersion curves and the corresponding normalized power fluxes for the TM-like SP modes of the DDMTM subwavelength hole with a 20.0 mm diameter. The SP mode solutions were all obtained within the ENG region (6 to 10 GHz) in Fig. 2, which corresponded to the case in Fig. 3(c). While the TM_{0n} mode ($m = 0$) only had backward waves with a negative slope in the dispersion curves, the hybrid modes ($m \geq 1$) exhibited both forward and backward waves, as shown in Fig. 6(a). For the previous EH_{m1} mode when $D = 20.0$ mm , the modes were only backward type. As in the previous TE-like mode cases, no backward waves existed below the critical frequency of $f = 7.071$ GHz , corresponding to point "*B*" in Fig. 2, where $\varepsilon_{r2} = -1.0$. In contrast, forward waves were found to exist below and above the critical frequency. The TM-like SP modes were also monomodal, *i.e.*, there

#7129 - $15.00 US
Received 12 April 2005; revised 1 May 2005; accepted 1 May 2005

were no higher order modes. The cutoff frequencies, *i.e.*, the frequencies at $\beta / k_0 = 1.0$, for the TM_{01}, HE_{11}, and HE_{21} modes were 7.695 GHz, 6.923 GHz, and 6.967 GHz, respectively.

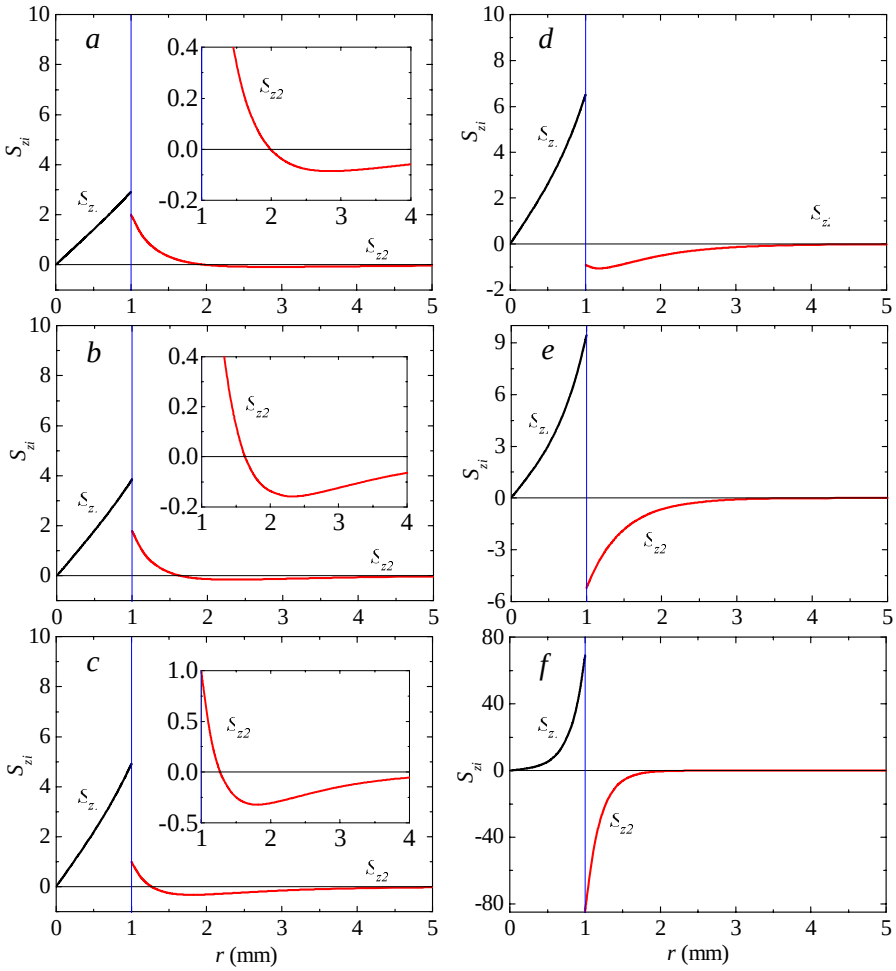

Fig. 8. Spatial power distributions of Poynting vectors S_{z1} and S_{z2}. Amplitude is an arbitrary unit .

Since the bifurcation frequency between the forward and backward waves of the HE_{11} mode was 7.344 GHz, which was higher than the cutoff frequencies for the hybrid modes, the single TM_{01} mode propagation region spanned from 7.344 to 7.695 GHz with a width of 0.351 GHz. The obtained operating wavelengths ranged from 23.08 mm (6.923 GHz) to 38.99 mm (7.695 GHz) when the diameter of the hole was 20.0 mm. Figure 7 shows the dispersion curves and normalized power fluxes of the TM-like SP modes for the DDMTM subwavelength hole with a 2.0 mm diameter. The cutoff frequencies for each SP mode shifted toward higher frequencies when compared with the case of $D = 20.0$ mm. For example, they were 9.812 GHz and 7.115 GHz for the TM_{01} and HE_{11} modes, respectively. Due to the bifurcation character of the hybrid HE_{m1} modes, the bifurcation frequency of the HE_{11} mode was 7.658 GHz, which was higher than the cutoff frequency observed in the previous cases. Thus, the

#7129 - $15.00 US
Received 12 April 2005; revised 1 May 2005; accepted 1 May 2005

single TM_{01} mode operation region became broader than in the case of $D = 20.0$ mm, *i.e.*, 7.658 to 9.812 GHz, where the width was 2.154 GHz. The operating wavelengths ranged from 30.57 mm (9.812 GHz) to 42.42 mm (7.071 GHz), representing approximately 15 to 20 times the 2.00 mm diameter of the subwavelength hole. In the hybrid mode cases, the normalized power flux η increased when compared to the case of $D = 20.0$ mm, indicating that the power flux of the mode was more confined, and η even became unity below a certain critical frequency. For the HE_{11} mode, $\eta = +1$ below 7.32 GHz (point *b*), as shown in Fig. 7 (b). The $\eta = +1$ value indicates that the direction of the power flux in the DDMTM region was parallel to that in the free space region, which purportedly cannot be observed anywhere else. To find a more precise justification for this phenomenon, the spatial power distributions in a cross-section of the subwavelength DDMTM hole were investigated using the Poynting vectors S_{z1} and S_{z2}, as shown in Fig. 8, at the points marked in Fig. 7. At points *a* ($f = 7.25$ GHz), *b* ($f = 7.32$ GHz), and *c* ($f = 7.40$ GHz), S_{z2} was positive near the interface between the DDMTM and the free space, even though S_{z2} was the Poynting vector for the MTM region. However, S_{z2} became negative again as r increased. At point *a*, the integration of the positive portion of S_{z2} was larger than that of the negative portion. Thus, η became +1 due to $P_2 > 0$. The onset of this phenomenon occurred just below point *b*, where the integrations of the positive and negative portions of S_{z2} cancelled each other, and $P_2 = 0$. This $\eta = +1$ propagation was also found in the hybrid SP mode with sufficiently small hole radii. However, at point *c*, the integration of the negative portion of S_{z2} was dominant over the integration of the positive portion, where $P_2 < 0$ and $\eta < 1$. At points *a*, *b*, and *c*, it should be noted that the border of the counter-propagation between the forward and backward Poynting vectors was located within the MTM region. This is essentially different from the Poynting vector fields previously found in MTM slabs [14, 31] or ground MTM slabs [20], where the counter-propagation of the Ponting vectors between the MTM region and the conventional dielectric region are always at the interface. Therefore, the distinctive counter-propagation phenomenon was surely associated with the hybrid modes in the circular guiding cross-section, plus the effect of a small-sized hole. At higher frequencies, *e.g.*, *d* ($f = 7.50$ GHz), *e* ($f = 7.60$ GHz), and *f* ($f = 7.60$ GHz) in Fig. 7, the positive portions of S_{z2} near the surface disappeared and S_{z2} remained negative at all positions, as usually expected. Although we considered an infinite MTM cladding, the amount of power flow even at some distance from the hollow core boundary is very negligible, as seen from Fig. 8. For example, in the case of 2.0 mm diameter hole, at 5.0 mm from the center of the hollow core, the power level is extremely low, which can be considered as to be zero. Besides, the operating wavelengths are larger than the diameter by 15 to 20 times in this case. So, the hollow cylinders of the MTM cladding with finite thickness can also be analyzed in the present simple method. Lastly, the HE_{m1} mode was more tightly bound than the EH_{m1} mode when the normalized power fluxes of both modes in Figs. 4-7 were compared with each other.

4. Conclusions

This work investigated the electromagnetic dispersion and power flux characteristics of DDMTM holes with two different subwavelength diameters. TE-like and TM-like SP modes were both found to exist, and only the principal modes for each azimuthal eigenvalue had proper solutions. The obtained TE-like and TM-like SP modes were within the frequency region of the DNG and ENG, respectively. Two critical frequencies were identified for the lower limits of the backward TE-like and TM-like modes, where $\mu_{r2} = -1.0$ and $\varepsilon_{r2} = -1.0$, respectively. Nonetheless, the TM_{01} and TE_{01} modes only supported backward waves, while the hybrid modes supported both forward and backward wave modes, thereby generating a

#7129 - $15.00 US Received 12 April 2005; revised 1 May 2005; accepted 1 May 2005

frequency region where two or three orthogonal modes could coexist. In particular, forward waves appeared for the EH_{m1} mode when the radius of the hole was small. Meanwhile, the HE_{m1} mode with a small-sized hole exhibited a distinctive counter-propagation of the Poynting vectors in each region, which was the main reason for the $\eta = +1$ propagation.

The analysis presented here may find an application such as a prove tip of near-field microscope which can operate in two polarization modes, simultaneously or independently.

The present study may help in understanding the enhanced transmission phenomena, which can be observed in the subwavelength hole structure of finite length surrounded by the MTM.

Acknowledgments

This work was supported by grant No. R01-2004-000-10158-0 from the Basic Research Program of the Korea Science & Engineering Foundation.

#7129 - $15.00 US Received 12 April 2005; revised 1 May 2005; accepted 1 May 2005